EARTHQUAKE ENGINEERING AND STRUCTURAL DYNAMICS
Earthquake Engng Struct. Dyn. 2017; **46**:561–583
Published online in Wiley Online Library (wileyonlinelibrary.com). DOI: 10.1002/eqe.2803

Earthquake risk assessment of buildings accounting for human evacuation

Alan Poulos[1], Juan Carlos de la Llera[1,*,†], Judith Mitrani-Reiser[2]

[1] *Department of Structural and Geotechnical Engineering, Pontificia Universidad Católica de Chile, and National Research Center for Integrated Natural Disaster Management CONICYT/FONDAP/15110017, Santiago 7820436, Chile*
[2] *Department of Civil Engineering, Johns Hopkins University, Baltimore, MD 21218, USA*

SUMMARY

A primary goal of earthquake engineering is to protect society from the possible negative consequences of future earthquakes. Conventionally, this goal has been achieved indirectly by reducing seismic damage of the built environment through better building codes, or more comprehensibly, by minimizing seismic risk. However, the effect that building damage has on occupants is not explicitly taken into account while designing infrastructure. Consequently, this paper introduces a conceptual framework and numerical algorithm to assess earthquake risk on building occupants during seismic events, considering the evacuation process of the structure. The framework combines probabilistic seismic hazard analysis, inelastic structural response analysis and damage assessment, and couples these results with the response of evacuating agents. The results are cast as probability distributions of variables that measure the overall performance of the system (e.g., evacuation times, number of injured people, and repair costs) for specific time windows. As a testbed, the framework was applied to the response of a reinforced concrete frame building that exemplifies the use of all steps of the methodology. The results suggest that this seismic risk evaluation framework of structural systems that combine the response of a physical model with human agents can be extended to a wide variety of other situations, including the assessment of mitigation actions in communities and people to improve their earthquake resilience. Copyright © 2016 John Wiley & Sons, Ltd.

Received . . .

KEY WORDS: risk assessment; evacuation model; agent-based modeling; performance-based engineering; human-structure interaction.

1. INTRODUCTION

The annual estimated average economic loss between 2005-2014 attributed to the direct damage caused by global earthquakes is US$ 43 billion, and the annual average population affected is 8.4 million during the same period [1]. It is apparent that one outstanding factor in these consequences is the increase in population and urbanization due to accelerated economic growth, and the ways people and communities interact with the built and natural environment [2]. These costly effects, added to the possibility of stakeholders to better understand and select performance levels of structures, has driven earthquake engineering to venture in performance-based design. In this sense, the Pacific Earthquake Engineering Research Center (PEER) has developed a robust probability-based framework for Performance-Based Earthquake Engineering (PBEE) [3, 4, 5], which enables risk assessment of physical systems. The methodology has been used in numerous previous studies

*Correspondence to: Juan Carlos de la Llera, Department of Structural and Geotechnical Engineering, Pontificia Universidad Católica de Chile, Av. Vicuña Mackenna 4860, Santiago 7820436, Chile.
†E-mail: jcllera@ing.puc.cl

to estimate the seismic risk of a wide range of physical systems such as buildings and bridges [6], as well as applied to other hazards such as buildings under fire [7].

However, earthquake-induced damage of buildings affect occupants, causing injuries, deaths, and other psychological effects, such as post-traumatic stress disorder and depression [8]. This interaction between buildings and human response is not commonly modeled when estimating human risk variables, and the latter normally come from empirical data reliable only at a regional scale [9]. To enable the calculation of interacting physical and human response variables, this investigation integrates and implements in the probability framework developed by PEER, the interaction of people and their physical environment using Agent-Based Modeling (ABM) [10], a powerful simulation technique in which a system is conceived as a collection of autonomous decision-making entities called agents interacting among them and with their environment.

This work presents a conceptual and numerical framework that computes the risk that the occupants of a specific building face in seismic events, and applies this methodology to the evacuation of a real reinforced concrete frame building located in the city of Santiago, Chile, which is used as a testbed. A general overview of the steps in risk assessment is presented in Figure 1. The model uses Probabilistic Seismic Hazard Analysis (PSHA) to characterize the seismic hazard at the building's location; an inelastic structural model of the building to obtain the response to ground motions that represent its seismic hazard; fragility analysis to link structural performance metrics (e.g., inter-story drifts and floor accelerations) with damage of non-structural components; and an ABM of human evacuation, which includes the interaction between agents and their damaged physical environment due to earthquake loads. The human-physical interactions considered in the model are: injuries due to falling of non-structural components, increase of agent stress levels, reduction in agent speed, and other changes in the motion of agents that are associated with a damaged scenario. The results of the model are cast as probability distributions of global output variables (e.g., evacuation times, injuries, and repair costs) during a period of time that could be the lifetime of a building. These results could help in better preparing and mitigating the eventually devastating consequences on buildings and people when they are subjected to extreme earthquake motions.

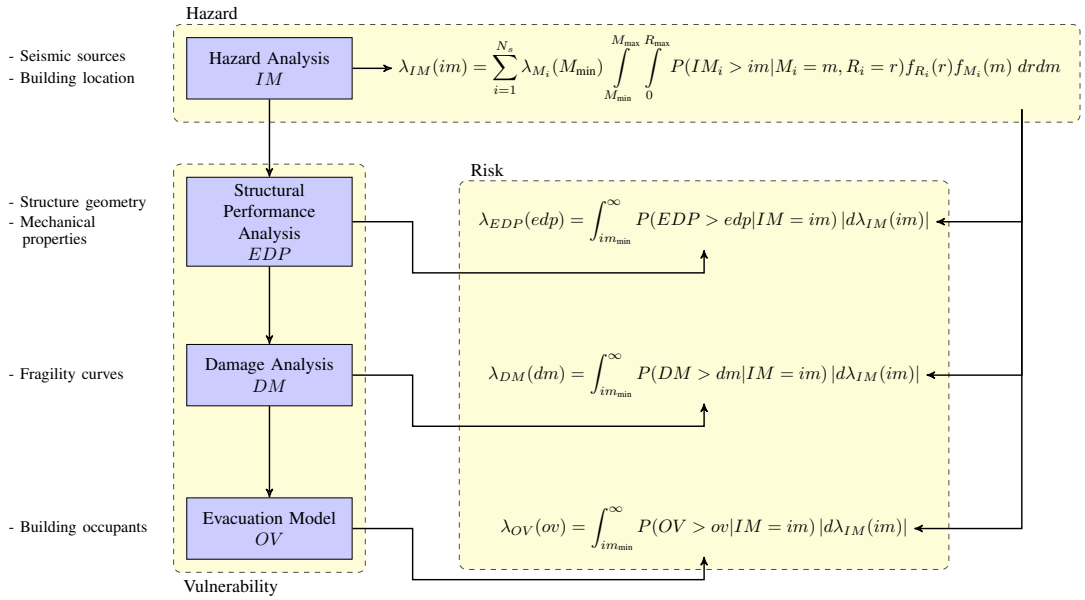

Figure 1. Schematic overview of the framework for risk evaluation.

It is apparent that the inelastic response of the structure may influence the evacuation process of the building occupants due to structural and non-structural damage, and that this interaction only applies in this cascading direction. Therefore, the two problems, i.e. the inelastic structural response

DOI: 10.1002/eqe.2803

and the building evacuation, may be considered one after the other as indicated in Figure 1. The existing literature on each computation module of Figure 1 is vast. On the other hand, the literature on the central purpose of this investigation, which is the human-structure interaction problem, is almost non-existent, and the strategy followed by the authors is to present throughout the article the most significant references and ideas in the different subjects areas, as they are needed.

2. EVACUATION MODEL

Human evacuation was simulated using ABM, a bottom-up computational technique that conceives a system as multiple decision-making entities called agents, representing, in this case, people. ABM enables the emergence of complex global behaviors from simple behavioral rules at the agent level. The agent-based model used to simulate evacuation in this work is adapted from the one described earlier in [11], and was implemented in Netlogo [12], a multi-agent programmable modeling environment. Just for the sake of completeness, the original model will be briefly explained here.

The physical setting where the evacuation takes place, in this case the building spaces, is first transformed into a graph. The shortest path to each vertex of the graph is computed using Dijkstra's Algorithm [13]. At every time step, each agent finds a global path following the vertex that minimizes the distance to the exits of the building. Agents set their preferred velocity pointing to these vertices, and after the computation of these preferred velocities, the optimal reciprocal collision avoidance principle (ORCA) [14] is imposed to modify velocities and ensure no collision among agents and with static objects (e.g., walls and furniture). Finally, these velocities are used to update the position of all agents. Other social behaviors of agents such as joint evacuation (grouping) and following surrounding agents (herding) were studied and included in the original model; however, they will not be considered in this drill since agents knew each other and were instructed on how to evacuate.

This evacuation model was validated with a drill performed in a K-12 school in the city of Iquique, Chile, were approximately 1500 people took part in the evacuation. The results of the model agreed well with the evacuation drill [11]. An evacuation drill was also performed in the office building described herein on July 24$^{\text{th}}$, 2014. The evacuation of 200 people was completely recorded using video cameras. The cumulative number of evacuees as a function of time (evacuation curve) obtained from 30 simulations of the model and the real drill results are compared in Figure 2a, showing again excellent agreement between modeled evacuation data and the actual evacuation process.

The evacuation model can be applied to different types of buildings and numbers of people, as evidenced by the two successful validations (K-12 school and office building). However, in both cases the initial conditions of the agents, i.e., pre-evacuation times and initial positions, were estimated or directly obtained from the video recordings. This information, however, will not be available in predicting future evacuations, and must be generated by the model. As a way to show what would happen if this uncertainty is introduced, this current drill was simulated again by randomly spatially distributing the 200 agents across the building using a uniform distribution, and assuming that the pre-evacuation time of people follows a Weibull distribution as obtained previously for the school's drill (scale parameter $\alpha = 1.63$ and shape parameter $\beta = 50$) [11]. Results shown in Figure 2b indicate that the simulated evacuation curves are clearly shifted by about 30 s relative to the real drill, though the shapes of the curves are roughly the same. The difference in pre-evacuation time is explained by the fact that the sirens were heard with considerable delay by some people. Future studies could be carried out to determine if this difference is due to the chosen pre-evacuation time distribution, or to other specific characteristics of the drill.

A different agent-based model considering the effect of non-structural damage on the evacuation of human agents has been studied earlier [15]. This previous model defines the state of the building before evacuation begins. However, due to the long duration (several minutes) of Chilean subduction earthquakes, or earthquake aftershocks, damage of non-structural components may occur during an evacuation process. This is also the case for many other disasters in which people need to evacuate in an environment that changes in real-time as a result of the disaster. Thus, the model uses real-time

DOI: 10.1002/eqe.2803

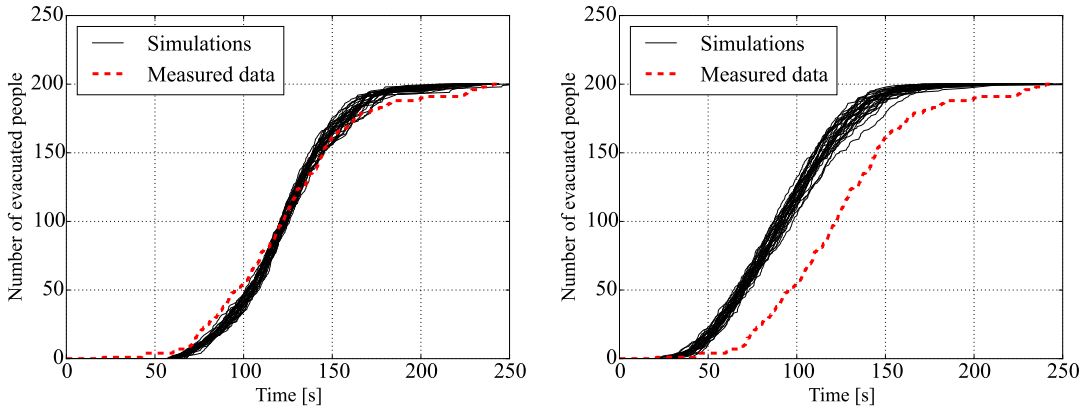

(a) Using real pre-evacuation times

(b) Predicting pre-evacuation times

Figure 2. Evacuation curve of the testbed building drill.

damage of non-structural components to modify two agent variables: health and stress; values for both variables range between 0 and 1, with health starting at 1 and stress at 0. The assumptions next for the ABM are exclusively based on intuition, and some degree of past experience on evacuation drills, but they require in the future to be validated further using experimental data. Future research can be carried out using formal psychological and neuro-scientific tests that help answer research questions such as: What makes a person start evacuating spontaneously?; How can we better quantify the effect that building damage has physically and psychologically on health and stress?; What is the relationship between stress and the different behavioral regimes of a person?; How much does the speed of a person increase when her/his behavioral regime changes?; How much does the average speed of a person decrease with varying severity and types of injuries?; What makes a person stop moving during an evacuation?; What is the speed of people walking on a pathway with debris caused by building damage?; etc.

Let us assume that if an agent sees moderate damage or collapse of a building component, its stress increases by 0.05 and 0.2, respectively. Also if a component (e.g., ceiling) collapses on an agent, its stress increases by 0.5 and its health factor is reduced by 0.5. Furthermore, it is assumed that the behavioral regime of an agent is determined by its stress level. All agents start the simulation in normal regime, and any increase in stress of an agent shifts its regime to rational. As agents enter a rational regime, they start evacuating (if they had not started before) and increase their preferred speed. Since the optimal rational response of each individual occurs at different stress levels [16], the stress limits between rational and panic regimes are assigned randomly for each agent using a standard uniform distribution $U(0,1)$. It is also assumed that agents in panic regime seeing collapse of a building component have a 50% probability to block and stop moving during a random interval between 5 to 10 seconds (uniformly distributed).

Therefore, the preferred speed of the i-th agent, used to compute its preferred velocity (Equation (2.3) in [11]), is influenced by various factors:

$$v_i^p = v_i^n f_i^s f_i^r f_i^d f_i^h \tag{1}$$

where v_i^n is the normal speed of the i-th agent, sampled from a Weibull distribution with mean 1.34 m/s (shape parameter 10.14, and scale parameter 1.41) that was calibrated previously using data from real evacuations [17]; f_i^s is a factor for speed reduction of agents on a staircase ($f_i^s = 0.5$) [18, 19]; factor f_i^r increases the speed if the agent is in rational or panic regime ($f_i^r = 1.3$); f_i^d is a factor to consider the speed reductions if the agent is walking on a pathway with debris (for collapsed non-structural components: $f_i^d = 0.5$ for partition walls, and $f_i^d = 0.7$ for suspended ceilings); and f_i^h is a factor to account for speed reduction of the agent following Equation (2), depending on health h_i, i.e.

$$f_i^h = (0.25 + 0.75 h_i) \tag{2}$$

DOI: 10.1002/eqe.2803

Moreover, individual agent pre-evacuation times are sampled from a probability distribution obtained from data taken from the school drill [11]. However, as explained previously, an agent may start evacuating before this instant of time if she/he enters the rational or panic regime. An effect that is not considered herein, which could be modeled in the future, is to assign agent speed equal to zero when a certain level of floor acceleration physically impedes agent movement.

Figure 3 illustrates the effect that building damage has on evacuating agents by showing four snapshots of a section of the fourth floor during a single simulation. The damage states of partition walls and ceilings are shown using different colors. The input ground motion used to assess building damage has intensity $Sa(T_f) = 0.77$ g and its north-south component is shown in the same Figure. At first, all agents are randomly positioned and are in normal regime. At t = 15 s the ground motion intensity has increased and generated significant damage in partition walls, which made some agents start evacuation and change their regime to rational or panic. After the peak ground acceleration has past, all building damage has already occurred and most of the agents started the evacuation (t = 30 s). Finally, at t = 45 s most agents are near the staircase and the floor is nearly empty.

As Figure 3 shows, agents start evacuating before the ground motion stops. This is largely based on empirical evidence from large earthquakes (e.g., Chile 2010) that have especially long duration (over a minute of strong ground motion). Immediate evacuation might be a good strategy in some particular cases, but mostly is a natural behavior of people in long earthquakes. Naturally, if the earthquake may trigger another consequential hazard, such as a tsunami or a fire, it may be reasonable to expect such behavior. However, in some places immediate evacuation is not recommendable because it exposes people to falling objects, and docking under furniture would represent a safer condition. Please note that we do not advocate for any particular evacuation strategy, and it is by the use of the proposed models that the better strategy can be defined and quantified.

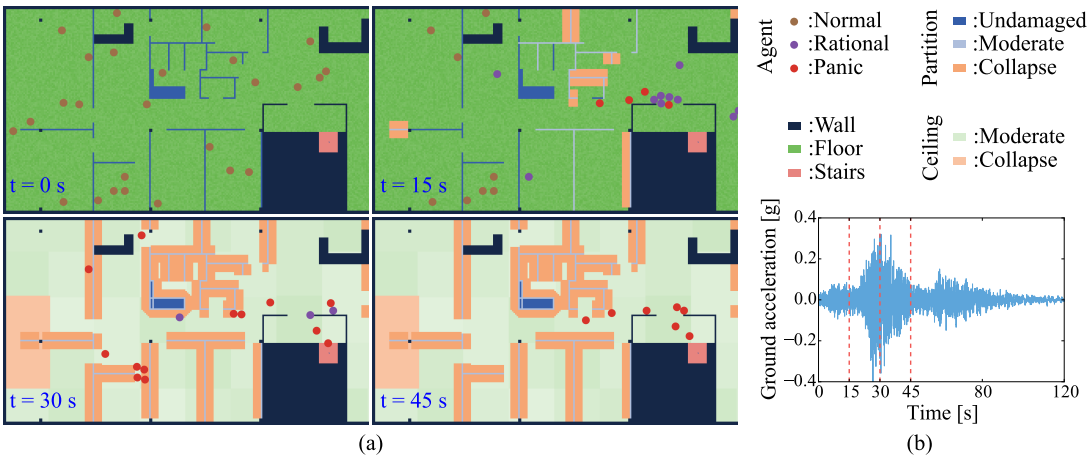

Figure 3. Example of a single evacuation simulation: (a) snapshots of a portion of the fourth floor at times t = 0, 15, 30, and 45 s; and (b) north-south component of the input ground motion.

3. GENERAL FORMULATION OF THE RISK PROBLEM

The risk evaluation problem is presented in a schematic way in Figure 1. This figure includes the relevant equations that are needed and is structured in three main blocks: hazard, vulnerability, and risk. The structure presented will be used in this article to describe in more detail the most relevant conceptual and implementation aspects of this framework. Most of the equations presented are well described in the literature, however, for the sake of completeness we have preferred to reproduce them in this diagram. Moreover, some of them require careful interpretation, which is included herein.

DOI: 10.1002/eqe.2803

The central equation that governs the risk evaluation problem may be written as a generalization of the usual PBEE framework [4, 5]:

$$\lambda_{OV}(ov) = \int_{im_{\text{min}}}^{\infty} P(OV > ov|IM = im)\,|d\lambda_{IM}(im)| \tag{3}$$

where OV represents any output variable; IM is the local intensity measure of the earthquake; im_{min} is smallest relevant intensity measure, defined as the largest value of the intensity measure that has no engineering significance; $\lambda_X(x) = \nu P(X > x)$ is the mean annual rate of an arbitrary variable X exceeding the value x; λ_{IM} is the hazard curve; ν is the mean annual rate of significant events ($\lambda_{IM}(im_{\text{min}})$); and $P(OV > ov|IM = im)$ is the probability that random variable OV exceeds ov given the occurrence of an event with intensity $IM = im$. Output variable OV is equivalent to the decision variable DV used extensively in seismic risk literature, however we have deliberately changed the name and notation of this variable to reduce the confusion with the well-known definition used in optimization, i.e. variables that the decision maker controls (e.g., structural design). Equation (3) combines the seismic hazard at the building location with the vulnerability of the system to assess its risk. Once λ_{OV} is known, it is straight forward to compute almost any other statistics and probability distributions by assuming that the occurrence of significant events follow a Poisson process. Therefore computation of λ_{OV} is a critical step in the evaluation of risk. Indeed, since

$$F_{OV}(ov) = P(OV \leq ov) = 1 - P(OV > ov) = 1 - \frac{\lambda_{OV}(ov)}{\nu} \tag{4}$$

and

$$f_{OV}(ov) = \frac{d}{d(ov)} F_{OV}(ov) = -\frac{\lambda'_{OV}(ov)}{\nu} \tag{5}$$

it is possible to compute the CDF and PDF of the output value OV directly from λ_{OV} and its derivative.

Although for a subduction zone we know that any future earthquake will occur at the plate interaction boundaries, the extension of this fault is the whole country and we never know exactly the magnitude and source-to-site distance. Therefore, we need to sample these variables stochastically. Furthermore, the Poisson recurrence model assumes temporal and spatial independence, and it is widely known that this assumption limits the capacity to represent regional seismicity in some cases. However, the fit to the Poisson model improves as the number of discrete sources increases since the sum of any number of random point processes tends to a Poisson process [20]. This work uses the Poisson model since it is the most commonly used earthquake recurrence model, and because, as far as the authors know, no other type of model has been developed to represent Chilean seismicity more precisely.

Before getting into the details of how the human evacuation model is integrated within the risk model described by Equation (3), it is useful to examine the pseudo-algorithm presented in Figure 4, which shows the iteration process needed to estimate the evacuation response of the building occupants for a given intensity level im_i. The reader will find this Figure useful to better understand the following sections. First, a ground motion that matches the selected intensity is used as the input of the building inelastic model to obtain the dynamic response of the structure. The damage states of all non-structural components and the times when they are reached are computed with the sampling procedure explained in the previous section, and define the damaged setting of the field that will be used for the evacuation. On the other hand, the evacuation model is set up by sampling the stochastic properties of the agents (e.g., their position in the building plan and their speed). Then, a run of the evacuation model is done and the values of the selected output variables stored. The simulation is repeated N times, by sampling at each time the non-structural damage and agent parameters. The complete procedure is performed for M ground motions to finally obtain the probability distribution of the output variables at the selected intensity level.

DOI: 10.1002/eqe.2803

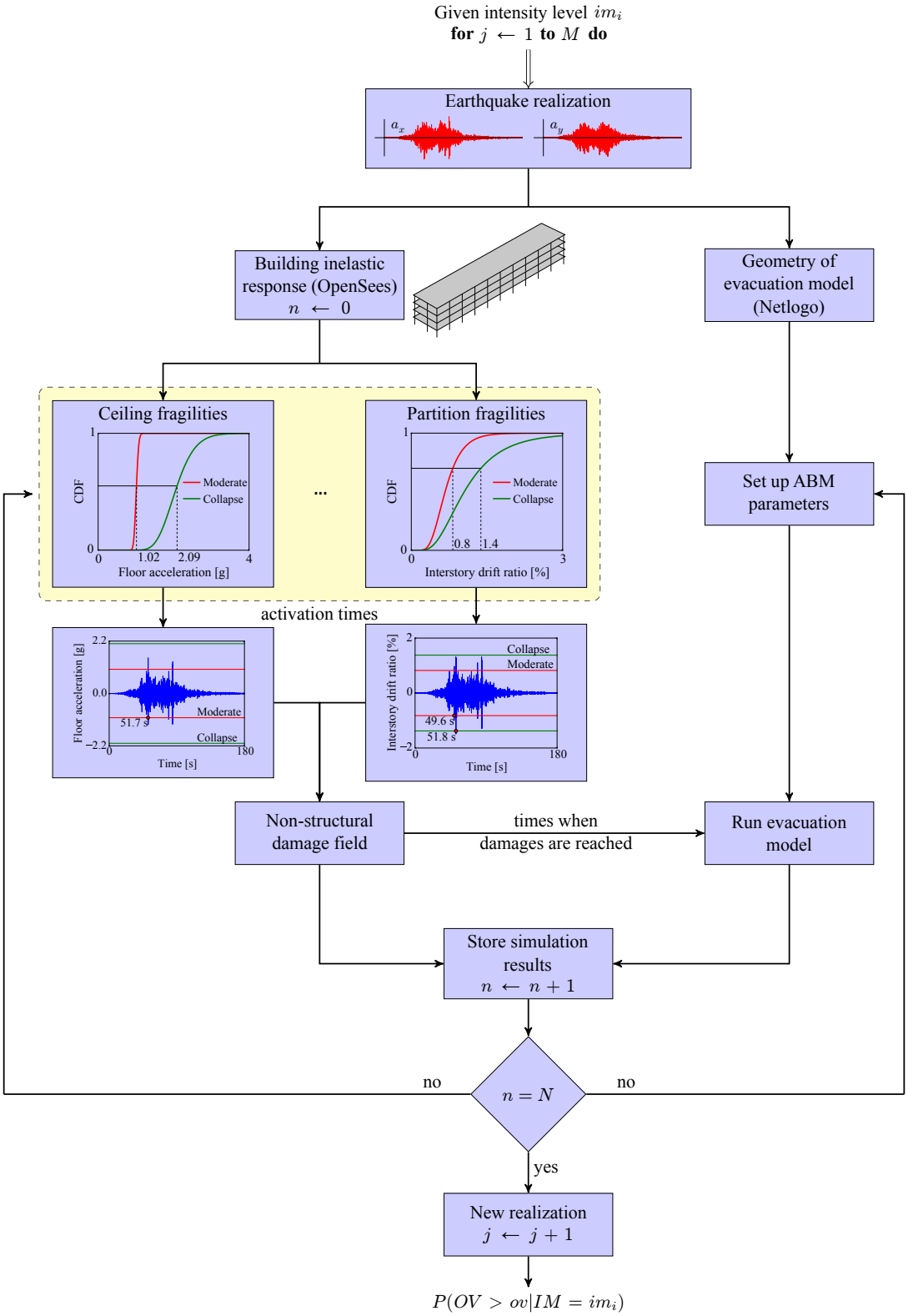

Figure 4. Schematic overview of evacuation vulnerability assessment.

DOI: 10.1002/eqe.2803

4. SEISMIC HAZARD

As shown in the flow diagram presented in Figure 1 and Equation (3), it is essential to characterize first the hazard field. The seismic hazard of a site is calculated using PSHA [21]. This technique estimates the probability of occurrence of all the possible seismic events at a site by estimating the mean annual frequency of events λ_{IM} that generate a ground motion which exceeds a certain intensity measure (im), conditioned on earthquake magnitude M and source-to-site distance R. The IM selected for this work is the spectral acceleration at the fundamental period of the structure $Sa(T_f)$, which, for short to moderate period structures, contains sufficient information of the excitation to help as a useful predictor of structural response [3].

In conventional PSHA, each seismic source is characterized by an annual number of earthquakes that exceed a given magnitude $M = m$. The statistical trend follows the well-known Gutenberg-Richter law [22], where $\lambda_M(m) = 10^{a-bm}$ is the mean annual frequency of earthquakes such that $M > m$, and coefficients a and b are estimated by regression analysis using historical data for a given homogeneous source. Events with magnitude smaller than M_{min}, say 5, have little engineering significance and are not included in the model. A source also has an upper bound magnitude M_{max}, say 9, which is the maximum earthquake it can generate. The Gutenberg-Richter law implies that the PDF of the magnitude M of earthquakes with $M_{\text{min}} \leq M \leq M_{\text{max}}$ is:

$$f_M(m) = \frac{b \ln(10) 10^{-b(m-M_{\text{min}})}}{1 - 10^{-b(M_{\text{max}}-M_{\text{min}})}} \tag{6}$$

The seismic sources used to carry out this work are taken from reference [23], which subdivides the converging margin between the subducting Nazca and overriding South-American plate into coastal and interior planar faults with different geometric and G-R parameters as a function of latitude. More recent Chilean seismic recurrence models have also been presented, e.g. [24].

The mean annual frequency of intensity measure IM exceeding values im at a specific site is known as the hazard curve, and is obtained by adding the contribution of all independent seismic sources in the region, N_s, and conditioning to the different magnitudes M_i and source-to-site distances R_i, i.e.

$$\lambda_{IM}(im) = \sum_{i=1}^{N_s} \lambda_{M_i}(M_{\text{min}}) \int_{M_{\text{min}}}^{M_{\text{max}}} \int_{0}^{R_{\text{max}}} P(IM_i > im | M_i = m, R_i = r) f_{R_i}(r) f_{M_i}(m)\, dr dm \tag{7}$$

where $f_{M_i}(m)$ is given by Equation (6); $f_{R_i}(r)$ is the PDF of distances from the rupture plane to the site of interest, which usually assumes a uniform spatial distribution within the source; and R_{max} is the maximum distance of earthquakes considered in the analysis (beyond which motions are assumed to have no engineering consequences). The conditional probability $P(IM_i > im | M_i = m, R_i = r)$ is computed using a Ground Motion Prediction Equation (GMPE), which gives a prediction of the intensity measure (IM) produced by an earthquake at a given site, and its associated uncertainty. The GMPE used herein is that proposed by Abrahamson *et al.* for subduction zone earthquakes [25], which provides an estimate of the geometric mean horizontal component of spectral acceleration at different periods, considering a damping ratio of $\xi = 5\%$. The resulting hazard curve in the location of the testbed building located in Santiago, Chile, is shown in Figure 5a.

The information obtained from the hazard curve shown in Figure 5a is not enough to run dynamic analysis on a structure, since it only provides information on the spectral acceleration for a single fundamental period, T_f. However, by repeating this analysis at different periods, the hazard curves for spectral accelerations at other structural periods can be determined. These curves are also computed using Equation (7), but using a different period in the GMPE considered.

The spectral accelerations of the different hazard curves for a fixed mean annual frequency of exceedance correspond to a Uniform Hazard Spectrum (UHS) as shown in Figure 5b for each value of IM used in the hazard analysis. Each ordinate of a UHS has an equal exceedance rate λ, and hence, equal return period $T_r = 1/\lambda$. However, the UHS gives no insight on the simultaneous

DOI: 10.1002/eqe.2803

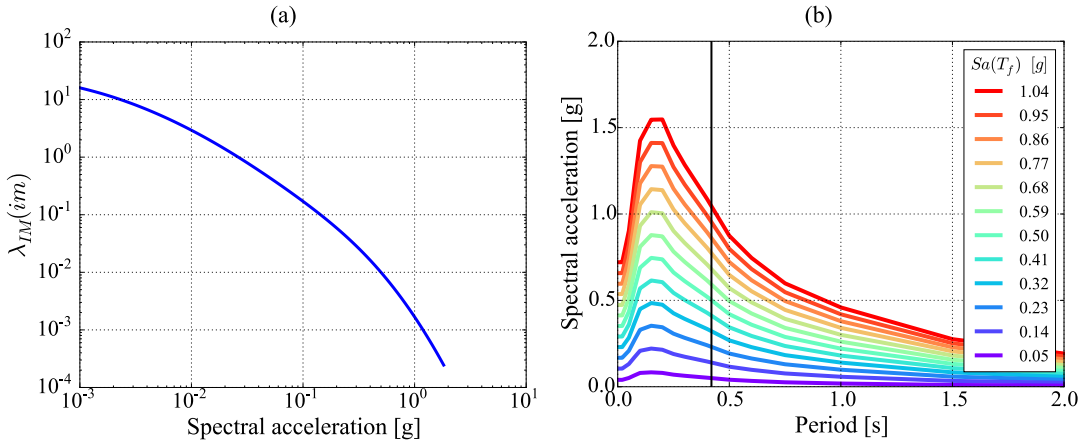

Figure 5. Characterization of the input ground motions: (a) hazard curve of the spectral acceleration at the fundamental period of the structure ($T_f = 0.42$ s); and (b) uniform hazard spectra for different values of IM.

exceedance of spectral accelerations at different periods, since they are normally caused by different earthquakes. The use of this spectrum as an input for structural analyses has been found to be conservative [26], and individual records with spectral accelerations as high as the UHS for all periods are physically unlikely. Alternatively, the simultaneous occurrence of spectral accelerations at different periods can be considered using the Conditional Mean Spectrum (CMS) [27]. However, CMS will not be used herein since it requires special calibration of correlation coefficients using regression analysis, which need to be specific for the region as explained elsewhere [28, 29]. Moreover, because the particular building considered is an old structure, the ductility of the system is limited and the conservative assumption of using the UHS could roughly represent the correct risk. Because the main goal of this work is to present the integrated methodology rather than parametric results with general applicability, the use of a UHS would be possible without limiting generality of the procedure.

However, since response spectra are still not enough to perform inelastic time history analysis on an inelastic structure, the selection and use of a suite of ground motion accelerograms is required to define the input at each intensity level. This was done in two ways: (i) by generating 4 spectrum-compatible ground motions derived using the guidelines explained elsewhere [30], but adapting the procedure to enable the construction of a pair of ground motions, whose spectral acceleration combined as a geometrical average lead to the UHS; and (ii) a set of 10 real records, scaled so that $S_a(T_f)$ matches the value selected. Records requiring a scaling factor greater that four to reach the selected intensity level were discarded. Both methods preserve the phase of the original records. The uncertainty in the phases of each record is not considered herein, and would increase the variability of structural response. The seed records of both methods were selected from real Chilean accelerograms recorded at sites with the same soil type as the one for the studied structure [31, 32], and come from earthquakes with magnitudes similar to the average magnitude obtained from seismic hazard deaggregation at the selected intensity level [33]. A list of the earthquakes that generated the selected ground motions for this work are presented in Appendix A. The Appendix also includes a range of the significant duration of the accelerograms, D_{5-95}, defined as the interval between the times at which 5% and 95% of Arias intensity ([34]) is reached.

5. STRUCTURAL MODEL AND DAMAGE ASSESSMENT

The second step in the algorithm presented in Figure 1 is the evaluation of the fragility and vulnerability of the physical system considered when subjected to the specified intensity measure IM. In this research, a four-story reinforced concrete frame building was selected. The building

DOI: 10.1002/eqe.2803

was built in 1968 and has a nominally symmetric building plan and the basic geometric properties presented in Figure 6. This structure hosts the headquarters of the school of engineering at PUC and one engineering department. An inelastic model of the structure was built using OpenSees [35], and the resulting stick model consists of inelastic fiber based frame elements aimed to characterize the inelastic behavior of the reinforced concrete sections of the structural members (beam with hinges element [36]). Building diaphragms are considered infinitely rigid in their plane, and provide no stiffness out-of-the plane. The fundamental period of the structure T_f is 0.42 s. This period defines the value of spectral acceleration used as IM.

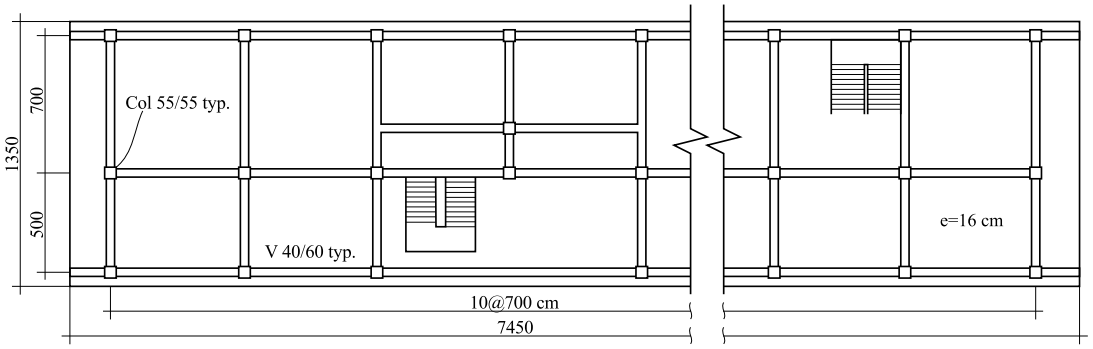

Figure 6. Second story building plan. All dimensions are in centimeters.

Apart from the inelastic behavior of the testbed structure, damage of non-structural components is dependent on the engineering demand parameters (EDPs). Typical parameters related to non-structural damage are interstory drift ratios and floor accelerations, depending on the type of component [9]. The testbed building has partition walls and suspended ceilings, which are drift- and acceleration-sensitive, respectively. Fragility curves, as the ones shown in Figure 7a, are used to assess the damage state of building components. These curves are obtained from experimental testing [37, 38] or analytical models [39], and are normally assumed to satisfy a log-normal distribution

$$f_X(x) = \frac{1}{x\sqrt{2\pi}\sigma}\, e^{-\frac{(\ln x-\mu)^2}{2\sigma^2}} \tag{8}$$

where parameters μ and σ are, respectively, the mean and standard deviation of the random variable $\ln(X)$, which is normally distributed. Table I shows the parameters of the fragility curves of each damage state limit for partition walls and suspended ceilings, which depend on interstory drift ratios and accelerations, respectively. The parameter x_m given in Table I is the median of the distribution, and is $\mu = \ln(x_m)$.

Table I. Fragility curve parameters and normalized repair costs of non-structural components.

Component	Damage state	x_m	σ	Norm. cost	Reference
Partition walls	Moderate	0.67%	0.39	0.2	[37]
	Collapse	1.05%	0.52	1.0	
Suspended ceilings	Moderate	1.01 g	0.051	0.2	[38]
	Collapse	2.04 g	0.200	1.0	

In each realization of a Monte Carlo simulation, the limits of the damage states are randomly sampled from the ordinates of fragility curves. The response of the corresponding EDP of each non-structural component is obtained from the dynamic model of the structure, and is used to find the time instant in which each damage state is reached, as shown in the example of Figure 7b. Repair costs of non-structural components are also shown in Table I, and are normalized by the total cost of replacing the component. For simplicity, all building components herein will be assumed to have

DOI: 10.1002/eqe.2803

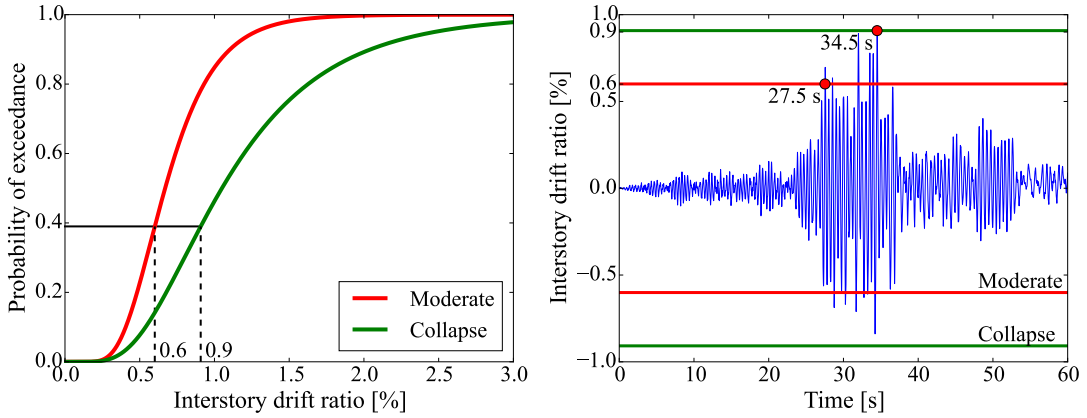

(a) Fragility curves of partition walls

(b) Response of the corresponding interstory drift ratio

Figure 7. Instants when the damage states of a partition wall are reached for a given probability of exceedance.

the same replacement cost, and hence the total repair cost is calculated simply as the sum of all damaged building components times the replacement cost.

6. INTEGRATED RISK EVALUATION

The integration of the dynamic analysis of the structure and the evacuation model enables us to compute output variables (OV) that involve the overall performance of the physical (structural) and human system (e.g., floor accelerations, downtimes, escape times, and injured people). The mean annual frequency of exceedance of an output variable, λ_{OV}, is estimated using Equation (3), where conditional probabilities $P(OV > ov|IM = im)$ are obtained from Monte Carlo simulations, using realizations of ground motions that match each intensity level considered (Figure 4). For example, Figure 8a shows the CDFs of the normalized building economic loss for different levels of earthquake intensity; analogously, the resulting mean annual frequency of exceedance λ_{OV} after integration of Equation (3) is shown in Figure 8b. These results were obtained using spectrum-compatible and scaled ground motions represented in the Figures by solid and dashed lines, respectively. Both ground motion selection methodologies resulted in similar loss curves, with scaled ground motions generally having more variance in the losses for a given intensity.

Equation (3) assumes that the system is restored to its initial state (i.e., that any damages of the building and its components are repaired) before the next earthquake occurs. This does not normally happen for aftershock sequences following a big event, since many ground motions strike a region in a relatively short period of time. Thus, the seismic risk methodology shown herein only considers mainshock events, i.e., seismic events that are temporally and spatially independent.

Human output variables, such as the number of injured people and evacuation times, are highly influenced by the occupancy level of the building. A simplified way of dealing with this fact is to consider only two mutually exclusive states for the structure: normal and zero building occupancy (e.g., nights and weekends). Let S be the event that an earthquake arrives when the building is occupied, and $P(S)$ its associated probability. Thus, the real exceedance probability is evaluated using the law of total probability conditioned to the occupancy level:

$$\begin{aligned} P(OV > ov|IM = im) = P(E) &= P(E|S)P(S) + P(E|\overline{S})P(\overline{S}) \\ &= P(E|S)\eta + P(E|\overline{S})(1-\eta) \end{aligned} \tag{9}$$

where $P(OV > ov|IM = im) = P(E)$ was used to simplify the notation; and η is the fraction of time that the building is occupied, chosen as 1/3 for the testbed building. However, the output

DOI: 10.1002/eqe.2803

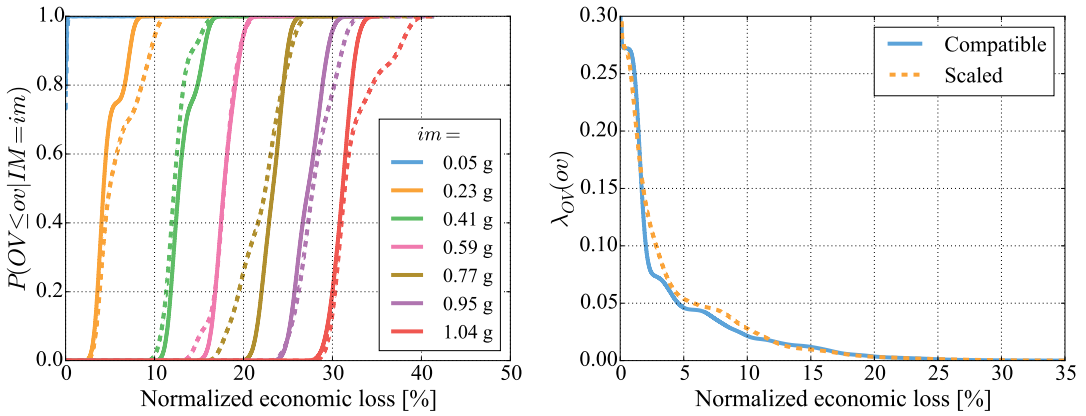

(a) Economic loss distribution for 7 of the 12 levels of earthquake intensity used

(b) Economic loss mean annual frequency of exceedance

Figure 8. Combination of seismic hazard and the vulnerability of the system to assess economic losses. Solid lines are results computed using spectrum-compatible ground motions and dashed lines are obtained with scaled ground motions.

variables will be typically zero (or minimal) when the building is empty, since nobody gets injured or is evacuated, thus simplifying the calculation to:

$$P(OV > ov|IM = im) = P(OV > ov|IM = im, S)\eta \tag{10}$$

The event $\{OV = ov\}$ given the occurrence of an earthquake characterized by $\{IM = im\}$ does not give information on the temporality of earthquakes and is not truly interesting to various stakeholder groups [5]. To cope with this difficulty, this work defines and studies two types of random variables that integrate the earthquake occurrence model with the results obtained from the PEER methodology, i.e. (i) the maximum value of an output variable in a certain time frame of t years, V; and (ii) the accumulated value of an output variable in a certain time window of t years, A. Output variables that represent loss on a system, such as casualties, economical losses, and downtimes, are more useful to stakeholders if calculated as accumulated values in a time window. Other variables that measure the performance of the system without representing a loss, such as escape times and EDPs, are not meaningful as accumulated values, and using their maxima V is more useful. The objective of this section is to calculate the distributions of both random variables from the $\lambda_{OV}(ov)$ curve, which requires defining the occurrence of seismic events as a stochastic process.

If the occurrence of earthquakes is assumed to be a Poisson process, as was first proposed by [40] and is commonly used in seismic hazard assessment, then the probability that n events will occur in a time window of t years is

$$P(N = n) = \frac{(\nu t)^n e^{-\nu t}}{n!} \qquad n = 0, 1, 2, ... \tag{11}$$

where ν is the mean annual number of significant events from all seismic sources ($\lambda_{IM}(im_{\text{min}})$). The probability that n events of intensity greater than im will occur in a time window of t years is also given by a Poisson distribution, with a qualified rate $\nu P(IM > im)$:

$$\begin{aligned} P(N_{IM}(im) = n) &= \frac{(\nu P(IM > im)t)^n e^{-\nu P(IM>im)t}}{n!} \\ &= \frac{(\lambda_{IM}(im)t)^n \, e^{-\lambda_{IM}(im)t}}{n!} \end{aligned} \tag{12}$$

DOI: 10.1002/eqe.2803

where $\lambda_{IM}(im) = \nu P(IM > im)$ is by definition the mean annual rate of exceedance of intensity measure $IM = im$. The same is also valid for any other random variable, in particular OV:

$$P(N_{OV}(ov) = n) = \frac{(\lambda_{OV}(ov)t)^n \, e^{-\lambda_{OV}(ov)t}}{n!} \tag{13}$$

The expected cumulative value of OV in one year, also known as expected annual loss, is simply the area under the λ_{OV} curve [41]

$$E[A, 1 \text{ year}] = \int_0^\infty \lambda_{OV}(\xi) d\xi = \nu E[OV] \tag{14}$$

Since Poisson processes are memoryless, the expected cumulative value for any time window t is directly proportional to t:

$$E[A, t] = t \cdot E[A, 1 \text{ year}] \tag{15}$$

If the output variable represents economic losses, a discount rate α should be considered as shown in Equation (16). This discount rate should not include inflation (i.e., real discount rate), since the considered repair costs are normally from the start of the time window.

$$E[A, t] = \int_0^t E[A, 1 \text{ year}] e^{-\alpha\tau} d\tau = \begin{cases} E[A, 1 \text{ year}] \dfrac{(1 - e^{-\alpha t})}{\alpha} & \text{if } \alpha > 0 \\ E[A, 1 \text{ year}] \cdot t & \text{if } \alpha = 0 \end{cases} \tag{16}$$

Equation (16) has been derived previously (e.g., [42, 43]), and only represent the mean value of the distribution of interest. An analytical procedure to obtain the full distribution is explained in Appendix B. The computational implementation of this approach may be challenging because of the multidimensional integration that is required. Alternatively, the distribution can be found numerically using many Monte Carlo simulations [43] as explained by Algorithm 1. Each trial generates a random sample of the number of events N_i in a certain time frame, samples a value of OV for each one of them, and adds up the OVs to obtain a sample of random variable A. Finally the cumulative probability of each sample A_i is estimated as the ratio between the trials that resulted in a value smaller than A_i and the total number of trials. Both, the analytic and the Monte Carlo methods were implemented and resulted in the same distributions shown in Figure 9b.

Algorithm 1: Monte Carlo simulations to find the distribution of cumulative variable A.

Data: Set the following parameters
M: number of Monte Carlo trials
t: time frame
α: discount rate ($\alpha = 0$ for no discount)
begin
  for $i \leftarrow 1$ **to** M **do**
    Randomly select a number of events N_i using the distribution in Equation (11)
    for $j \leftarrow 1$ **to** N_i **do**
      Randomly select a value of an output variable OV_j from the F_{OV} distribution of Equation (4)
      Randomly select a time of occurrence t_j from a uniform distribution $U(0, t)$
      $X_j \leftarrow OV_j e^{-\alpha t_j}$
    $A_i \leftarrow \sum_j X_j$
  Estimate the CDF as: $F_A(x) = \dfrac{1}{M} \sum_{i=1}^{M} \mathbf{1}(A_i \leq x)$, where $\mathbf{1}(\cdot)$ is the indicator function.

DOI: 10.1002/eqe.2803

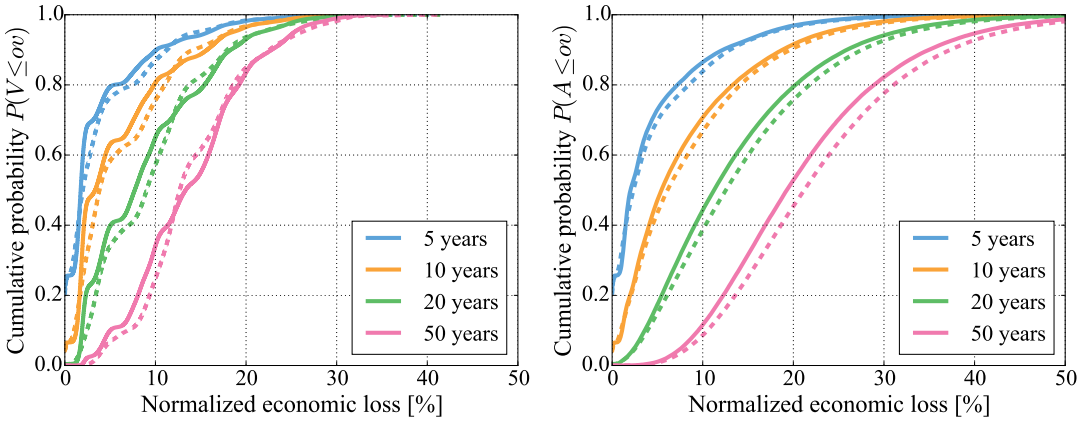

(a) Maximum value V (b) Accumulated value A

Figure 9. Example of CDFs of maximum and accumulated economic losses for different time frames. Accumulated values were obtained considering a discount rate $\alpha = 0.04$. Solid lines are results computed using spectrum-compatible ground motions and dashed lines are obtained with scaled ground motions.

The probability that the maximum value of an output variable in a time window of t years does not exceed ov is equivalent to the probability that no earthquake will generate values of the output variable greater than ov in that period, which is obtained by setting $n = 0$ in Equation (13), i.e.

$$F_V(ov) = P(V \leq ov, t) = P(N_{OV}(ov) = 0) = e^{-\lambda_{OV}(ov)t} \tag{17}$$

Appendix C shows how to calculate this distribution for an annual discount rate α. An alternative way to compute the distribution is using Algorithm 1, saving the maximum value of each trial instead of the accumulated value:

$$V_i \leftarrow \max_j X_j \tag{18}$$

and estimating F_V by the same counting procedure used to calculate F_A. Figure 9a shows the distributions of maximum economic losses for various time windows ranging from 5 to 50 years. An expected trend is that both random variables are similar for short time frames, but start to differ as the time frame increases. This is the case since for short time frames it is very unlikely to have more than one event with significant impact. It is important to note that random variables A and V have a mixed distribution (part discrete and part continuous), since the probability of them being zero is non-zero.

7. BUILDING RESULTS

A pseudo-code summarizing the necessary steps to calculate the probability distributions of output variables is shown in Algorithm 2. The Algorithm uses Monte Carlo simulations to compute the vulnerability of the system, and all of its steps are explained in previous sections of this article. This methodology was applied to the testbed building and used to compute distributions of four output variables: evacuation times, number of injured agents, number of agents who entered in the panic regime, and economic losses due to repair costs of non-structural components. Of these variables, only the last one does not depend on building occupancy. The rest are zero if the building is empty at the time of the earthquake. It is also important to point out that the repair cost variable does not include the human interaction aspects, and that the methodology assessment of its associated risk is known. However, such computation has been included in this work since it is needed to compute the rest of the output variables and because it shows the effect of using a discount rate.

All evacuation simulations considered 200 agents (the same as in the drill), which were randomly positioned throughout the building plan, and following a uniform distribution. The number of

DOI: 10.1002/eqe.2803

Algorithm 2: Methodological overview of risk assessment.

```
Data: Set the following parameters
[im_1, ..., im_L]: range of values of the intensity measure
M: Number of ground motions for each intensity measure
N: Number of simulations for each ground motion
begin
    Compute hazard curve λ_IM as explained in Section 4
    for i ← 1 to L do
        Calculate the UHS for intensity im_i
        Select M ground motions that are compatible with the UHS
        for j ← 1 to M do
            Run dynamic structural analysis on the building using ground motion j
            for k ← 1 to N do
                Sample fragility curves of non-structural components to obtain damage state limits
                Assess non-structural damage
                Run the evacuation model with the obtained damage
                Obtain the value OV_jk of the output variable
        Estimate P(OV > ov|IM = im_i) from all the OV_jk values
        Correct P(OV > ov|IM = im_i) by occupancy level as needed
    Use Equation (3) to obtain the mean annual frequency of exceedance of variable OV
    Follow the methodology of Section 6 to compute the maximum or accumulated distribution of OV
```

intensity levels used were $L = 12$ (linearly spaced between and including 0.05 g and 1.04 g). The minimum intensity was selected since it does not generate non-structural damage, and thus generating no economic losses nor effects over building occupants. The maximum intensity level is deemed acceptable to estimate the overall seismic risk since it only contributes 1-3% to the final results (Table II), and these contributions decrease with intensity level. A total of $M = 4$ spectrum-compatible ground motions were selected at each intensity. For each ground motion, a total of $N = 20$ simulations of the evacuation model were carried out. However, the economic loss was estimated using $N = 10000$, since it does not require the use of the evacuation model, which is computationally demanding. Additionally, the risk assessment of the economic losses was repeated using $M = 10$ scaled ground motions for each intensity.

The uncertainty in the Monte Carlo simulations used to compute the distributions of our output variables for a given intensity level (Figure 8a) originates from two sources, the selection of records and the sampling of fragilities. The former is somehow bounded since the records were made compatible or scaled to a target UHS. It would have been ideal to use also thousands of records, but since each of them requires an inelastic analysis of the structure, this is essentially impossible and justifies the use of a two-phase Monte Carlo strategy. However, the latter was obtained by sampling the fragilities 10000 times for a given ground motion, and leads to very small errors. For example, the estimated mean of the distributions of economic losses given a ground motion have less than 0.1% error.

A summary of the expected values and standard deviations of the calculated distributions for the testbed building is shown in Table II. These results were computed using spectrum-compatible ground motions. Mean accumulated values of the number of injured and panicked people are directly proportional to the considered time window (see Equation (16)), with small differences occurring due to the use of finite Monte Carlo simulations. However, the economic losses do not have this trend, since they were computed using a discount rate $\alpha = 0.04$. The mean value of maximum evacuation time is less sensitive to the time frame, especially for large time windows.

DOI: 10.1002/eqe.2803

Table II. Estimated mean and standard deviation (in parenthesis) of output variable distributions for the testbed building.

	Maximum	Accumulated		
Time frame (years)	Evacuation time (s)	Economic loss (%)	Injured	Panicked
5	185 (42.9)	4.37 (5.93)	0.94 (2.39)	6.4 (14.1)
10	207 (24.8)	7.98 (7.72)	1.89 (3.38)	12.9 (20.0)
20	220 (17.4)	13.3 (9.26)	3.77 (4.77)	25.8 (28.2)
50	231 (15.3)	21.1 (10.3)	9.42 (7.53)	64.6 (44.6)

The evacuation time is defined as the time between the start of an evacuation and the moment in which the last person exits the building. The distributions of the maximum evacuation time obtained for different time frames are shown in Figure 10a. The accumulated evacuation time in a time window is not shown since it is of little significance for decision making purposes. Figure 10b shows the evacuation time depending on the earthquake intensity level, which was calculated by averaging all simulations of the same intensity. An interesting observation of the evacuation model is that as the earthquake intensity level increases, the evacuation time initially decreases due to the fact that more agents enter the rational regime, which implies larger preferred speeds and makes agents start the evacuation. However, when the intensity exceeds a spectral acceleration of around 0.7 g, the evacuation time starts to increase, which is explained mainly by the slower movement of the agents due to building damage and the impact on agent's health condition. The shaded area of the Figure 10b represents one standard deviation, which increases with intensity due to a greater amount of building damage and agent response uncertainty.

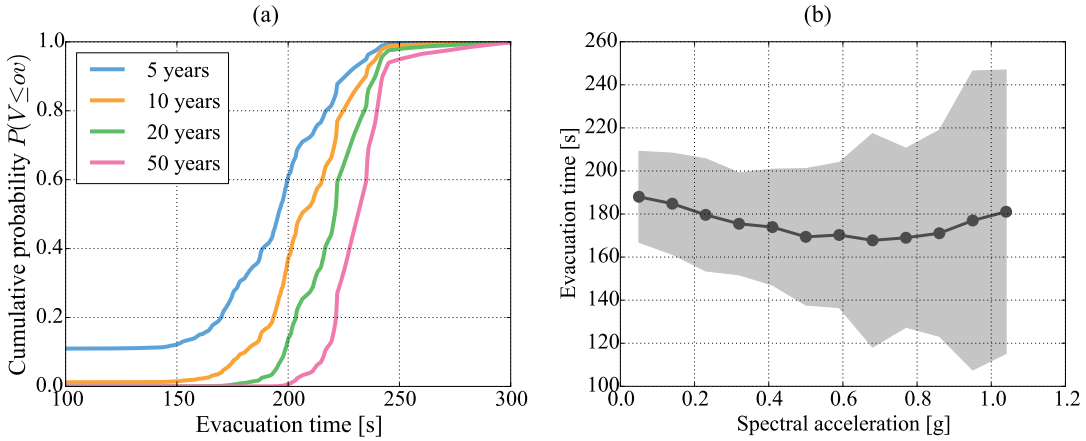

Figure 10. Total building evacuation time: (a) CDFs of maximum evacuation time (V) for different time windows; and (b) average evacuation time and plus/minus one standard deviation for each intensity level.

Economic losses originated from the cost to repair or replacement of non-structural components are considered in this analysis. Building contents, such as shelves, cabinets, electronic equipment, can also be considered similarly since they are acceleration-sensitive. The economic losses due to repair of structural components are not considered, but can be easily accounted for. Nowadays, the investment in the building construction phase of non-structural components and building contents is far greater than that of structural components, ranging from 82% to 92% [44]. The economic loss analysis does not require to run the evacuation model, which saves important computation time and enables the selection of a much higher number of Monte Carlo trials in Algorithm 2 (larger N). This increased number of Monte Carlo simulations decreases the error of the target distributions; the distributions obtained for the maximum and accumulated economic losses are shown in Figure 9, being the accumulated economic loss usually more meaningful for decision makers.

DOI: 10.1002/eqe.2803

The number of injured people was estimated simply as the total number of agents that were hit by falling non-structural components of the building according to the simulation results. This analysis does not provide any insight of the severity of the injuries; it only provides an estimation of the number of people that are physically affected by the earthquake. The cumulative distribution functions obtained for maximum and accumulated number of injured people are shown in Figure 11, being the accumulated value a more interesting result to assess risk on building occupants. As can be seen in the figure, the distributions are a step function since the random variable is discrete. The potential of such results is large and may lead to the need of serious improvements on a building's physical conditions, depending upon the number of injuries and the corresponding probabilities. Making more objective the number of injuries is a critical result for many decision makers.

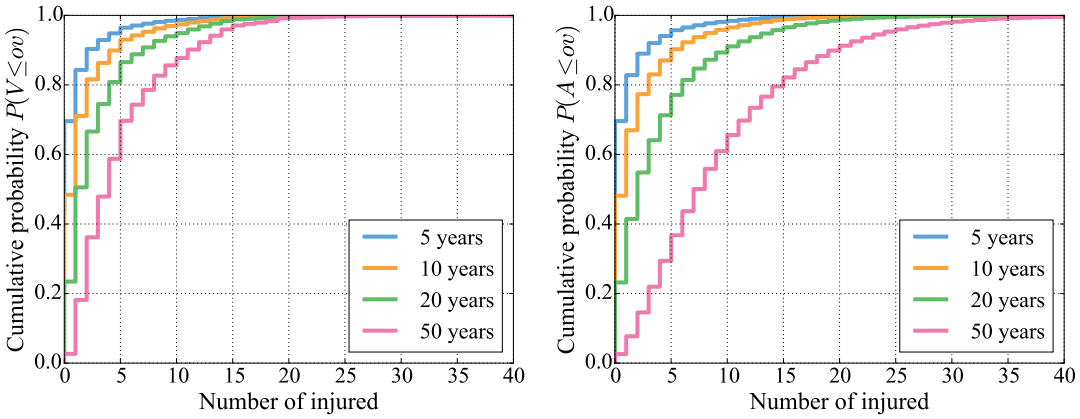

(a) Maximum value V (b) Accumulated value A

Figure 11. CDFs of maximum and accumulated number of injured people for different time windows.

Similarly, the number of panicked people was also obtained directly from the evacuation model, by counting the total number of agents that entered into the panic behavioral regime. Figure 12 presents the maximum and accumulated distributions for different time windows. The results show that more people enter in the panic regime than get injured, as can also be seen in the average values of Table II. As shown by these results, the possibility of combining the physical and human response enables us to compute very relevant information for decision makers, not only in terms of maximum values of physical quantities but rather distributions of physical and human output variables.

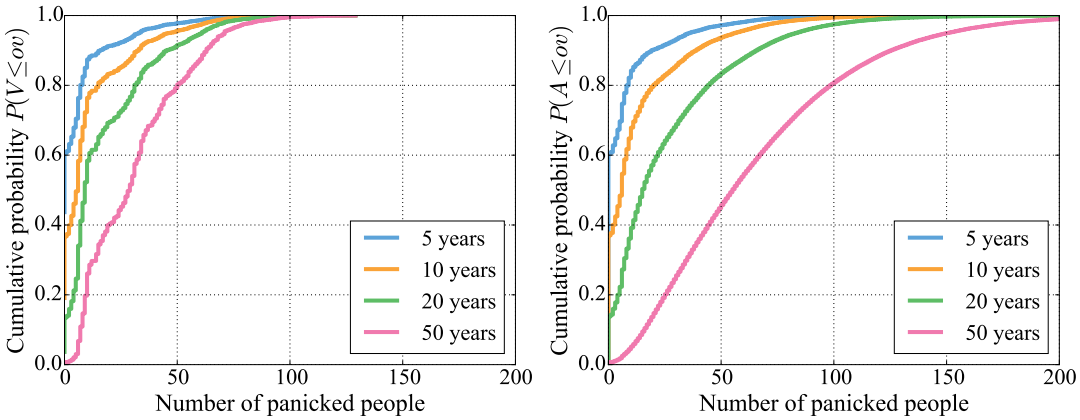

(a) Maximum value V (b) Accumulated value A

Figure 12. CDFs of maximum and accumulated number of people in panic for different time windows.

DOI: 10.1002/eqe.2803

8. CONCLUSIONS

This work proposes an integrated model to evaluate the risk of building occupants as the structure undergoes a large earthquake. As far as the authors know, this approach is novel and enables integration of the response of the structure and its components (physical system) with the evacuation of building occupants (social system) using the same probabilistic framework. To prove its efficiency, the framework was applied to a four-story reinforced concrete testbed building, resulting in probability distributions of output variables for different time frames. For example, for a time frame of 50 years in this building, the expected accumulated values of the output variables are about 9 injured people, 65 panicked people, and 21% economic loss as a ratio of the total repair cost. The expected maximum evacuation time from the building, in the same time window is 3.9 minutes. Consequently, the types of results obtained from this risk model can be very informative to emergency managers and help their decision making, thus helping in preparing and mitigating the eventually devastating consequences on buildings and their inhabitants as structures are subjected to extreme events, in particular, earthquakes.

This research has also led to closed-form expressions for the probability distribution of maximum and accumulated values of different risk output variables in a certain time window, which can be used in different contexts. All these expressions were validated using Monte Carlo simulations.

Some improvements that could be proposed to the methodology in the future are: (i) to change the target spectrum (UHS) used for ground motion selection to one that considers the joint probability of occurrence of spectral accelerations at all periods; (ii) to study the influence that the damage of structural components of the building have on agents; (iii) to develop a well grounded neuro-scientific based model to shed light on the decision making of agents, in particular, when they start evacuating; (iv) to study the effect that falling structural and non-structural components have on the health status of agents; (v) to prevent agent movement when a certain level of floor acceleration is reached; (vi) to consider in the analysis the economic losses derived from structural components and other building contents; and (vii) to add in the analysis other relevant human output variables, such as post-traumatic stress disorders.

The proposed model to assess risk of human agents during earthquakes can be extended to other hazards as well (e.g., fires, tsunamis, and floods), and also to other geographical scales (e.g., block, neighborhood, and city). Each different hazard requires to select specific intensity measures, assess their respective sources of uncertainty, and characterize the interaction between the human agents and the stressed surrounding environment.

APPENDIX A SELECTED EARTHQUAKES

Table III. List of earthquakes used for risk assessmet.

Date	Time UTC	M_w	Latitude	Longitude	Depth (km)	D_{5-95} (s)
1985-03-03	22:47:07	8.0	-33.240	-71.850	33.0	22.4 - 40.9
1985-04-09	1:56:59	7.2	-34.130	-71.620	37.8	11.6 - 33.3
1997-10-15	1:03:33	7.1	-30.933	-71.220	58.0	18.3 - 37.5
1998-01-30	12:16:08	7.1	-23.913	-70.207	42.0	21.8 - 22.3
2005-06-13	22:44:33	7.8	-19.987	-69.197	115.6	22.0 - 60.7
2007-11-14	15:40:50	7.7	-22.247	-69.890	40.0	46.9 - 53.2
2007-11-15	15:05:58	6.8	-22.925	-70.237	26.0	22.2 - 29.0
2010-02-27	6:34:11	8.8	-36.122	-72.898	35.0	40.0 - 51.6

DOI: 10.1002/eqe.2803

APPENDIX B PROBABILITY DISTRIBUTION OF ACCUMULATED LOSSES

The discounted value X of an economic loss due to a random earthquake that occurs in a time interval (window) of t years is

$$X = OVe^{-\alpha T} \tag{A1}$$

where α is the annual discount rate; OV is the economic loss, which follows the f_{OV} distribution; and T is a random variable that follows a uniform distribution $U(0,t)$, which has the following PDF:

$$f_T(\tau) = \begin{cases} 1/t, & \text{if } \tau \in [0,t] \\ 0, & \text{otherwise} \end{cases} \tag{A2}$$

Hence, the CDF of a discounted value can be obtained conditioning to the time when the earthquake occurs and using the total probability theorem:

$$\begin{aligned} F_X(x) &= \int_{-\infty}^{\infty} P(X \le x | T = \tau) f_T(\tau)\, d\tau \\ &= \frac{1}{t}\int_0^t P\left(OVe^{-\alpha\tau} \le x\right)\, d\tau \\ &= \frac{1}{t}\int_0^t F_{OV}\left(xe^{\alpha\tau}\right)\, d\tau \end{aligned} \tag{A3}$$

The CDF (F_X) and PDF (f_X) of the discounted value can be obtained numerically from this last Equation, since function F_{OV} is obtained from Equation (4).

The cumulative distribution function of the sum of discounted output variables (i.e., random variable A) in a time interval of t years can be obtained using the law of total probability and conditioning to the number of events n that occur in the time frame

$$F_A(ov) = P(A \le ov) = \sum_{i=0}^{\infty} P(A \le ov | N = i) P(N = i) \tag{A4}$$

where $P(N = i)$ is the probability that i events occur in the time interval, defined by Equation (11). For a case where i events occur, let $(X_j)_{j=1}^{i}$ define a sequence of random variables that represents the value of the discounted output variable X in each event. Each of these random variables follows the probability distribution f_X.

$$\begin{aligned} F_A(ov) &= P(n=0) + P(X \le ov)P(N=1) + \sum_{i=2}^{\infty} P\left(\sum_{j=1}^{i} X_j \le ov\right) P(N=i) \\ &= e^{-\nu t}\left[1 + F_X(ov)\nu t + \sum_{i=2}^{\infty} \frac{(\nu t)^i}{i!} P\left(\sum_{j=1}^{i} X_j \le ov\right)\right] \end{aligned} \tag{A5}$$

The probability distribution of a sum of random variables can be obtained by using the total probability theorem and conditioning to one of the variables:

$$\begin{aligned} P\left(\sum_{j=1}^{i} X_j \le ov\right) &= \int_0^{\infty} P\left(\sum_{j=2}^{i} X_j + X_1 \le ov | X_1 = x_1\right) f_X(x_1) dx_1 \\ &= \int_0^{\infty} P\left(\sum_{j=2}^{i} X_j \le ov - x_1\right) f_X(x_1) dx_1 \end{aligned} \tag{A6}$$

DOI: 10.1002/eqe.2803

Applying this procedure $i-2$ more times:

$$\begin{aligned} P\left(\sum_{j=1}^{i} X_j \leq ov\right) &= \underbrace{\int_0^\infty \dots \int_0^\infty}_{i-1 \text{ times}} P\left(X_1 \leq ov - \sum_{j=1}^{i-1} x_j\right) f_X(x_1)dx_1 \dots f_X(x_{i-1})dx_{i-1} \\ &= \underbrace{\int_0^\infty \dots \int_0^\infty}_{i-1 \text{ times}} F_X\left(ov - \sum_{j=1}^{i-1} x_j\right) f_X(x_1)dx_1 \dots f_X(x_{i-1})dx_{i-1} \end{aligned} \tag{A7}$$

The final distribution is found replacing this expression in Equation (A5):

$$F_A(ov) = e^{-\nu t}\left[1 + F_X(ov)\nu t + \sum_{i=2}^{\infty} \frac{(\nu t)^i}{i!} \underbrace{\int_0^\infty \dots \int_0^\infty}_{i-1 \text{ times}} F_X\left(ov - \sum_{j=1}^{i-1} x_j\right) f_X(x_1)dx_1 \dots f_X(x_{i-1})dx_{i-1}\right] \tag{A8}$$

Evaluating the distribution using this equation requires choosing a time interval t, discount rate α, and a hazard curve $\lambda_{IM}(im)$ (from which ν in obtained). Then λ_{OV} must be calculated using Equation (3), and replaced in Equations (4) to obtain F_{OV}. This result is then used in Equation (A3) to compute F_X and f_X. All these results are used in Equation (A8), where the infinite sum must be truncated when the contribution of the last value added to the partial sum is very small. It is convenient to compute the multidimensional integrals in Equation (A8) using Monte Carlo integration, which produces an error that is independent of the number of dimensions [45, 46], unlike typical numerical quadrature rules. This property, added to its easy implementation, makes Monte Carlo the method of choice for numerical integration in high dimensions.

APPENDIX C PROBABILITY DISTRIBUTION OF THE MAXIMUM LOSS

When the output variable, OV, represents an economic loss, a discount rate should be applied to account for the time cost of money. The discounted value Y of the economic loss due to an earthquake that occurs after τ years is

$$Y = OVe^{-\alpha\tau} \tag{A9}$$

where α is the annual discount rate. The CDF of random variable Y can be obtained directly from the OV distribution:

$$\begin{aligned} F_Y(y) &= P\left(Y \leq y\right) \\ &= P\left(OVe^{-\alpha\tau} \leq y\right) \\ &= P\left(OV \leq ye^{\alpha\tau}\right) \\ &= F_{OV}\left(ye^{\alpha\tau}\right) \end{aligned} \tag{A10}$$

The mean annual rate of seismic events that exceed a certain discounted value y is obtained analogously as in Equation (4):

$$\begin{aligned} \lambda_Y(y,\tau) &= \nu\left\{1 - F_Y(y,\tau)\right\} \\ &= \nu\left\{1 - F_{OV}\left(ye^{\alpha\tau}\right)\right\} \\ &= \nu\left\{1 - \left(1 - \frac{\lambda_{OV}(ye^{\alpha\tau})}{\nu}\right)\right\} \\ &= \lambda_{OV}\left(ye^{\alpha\tau}\right) \end{aligned} \tag{A11}$$

The mean annual rate of exceeding events decreases with time, since their associated economic losses become less important. This effect can be modeled by a non-homogeneous Poisson process,

Prepared using eqeauth.cls
DOI: 10.1002/eqe.2803

in which the probability that n events exceeding a discounted value of y will occur in a time interval of t years is

$$P\left(N_Y(y)=n,t\right)=\frac{\Lambda(y,t)^n e^{-\Lambda(y,t)}}{n!} \tag{A12}$$

where

$$\begin{aligned}\Lambda(y,t)&=\int_0^t \lambda_Y(y,\tau)\ d\tau\\&=\int_0^t \lambda_{OV}\left(ye^{\alpha\tau}\right)\ d\tau\end{aligned} \tag{A13}$$

Then the CDF of the maximum discounted value in a time interval of t years is calculated similarly to Equation (17):

$$F_V(v)=P(V\le v,t)=P(N_Y(v)=0,t)=e^{-\Lambda(v,t)} \tag{A14}$$

The final distribution for a specific time interval t and annual discount rate α is obtained by combining Equations (A14) and (A13):

$$F_V(v)=\exp\left(-\int_0^t \lambda_{OV}\left(ve^{\alpha\tau}\right)\ d\tau\right) \tag{A15}$$

where function λ_{OV} is obtained from Equation (3). If $\alpha=0$, Equation (A15) is the same as Equation (17).

NOMENCLATURE

M	Magnitude of an earthquake
R	Distance from the hypocenter of an earthquake to the site of interest
T_f	Fundamental period of the structure
IM	Local intensity measure of an earthquake (spectral acceleration at T_f for this study)
im_{min}	Minimum intensity measure used in the seismic risk analysis
$\lambda_X(x)$	Mean annual frequency of events with $X>x$, where X is a random variable
ν	Mean annual frequency of significant events ($\lambda_{IM}(im_{\text{min}})$)
EDP	Engineering Demand Parameter
DM	Damage Measure
OV	Output of the system when subjected to an earthquake
t	Time frame used in the risk analysis
A	Accumulated value of an output variable in t
V	Maximum value of an output variable in t
η	Fraction of time that the building is occupied
α	Real discount rate used for economic risk variables

ACKNOWLEDGEMENT

This research has been sponsored by the National Research Center for Integrated Natural Disaster Management CONICYT/FONDAP/15110017 and by Fondecyt grant #1141187. The authors are very grateful for this support.

REFERENCES

DOI: 10.1002/eqe.2803

1. Guha-Sapir D, Below R, Hoyois P. EM-DAT: The CRED/OFDA international disaster database. URL http://www.emdat.be, [accessed October 2015].
2. Neumayer E, Plümper T, Barthel F. The political economy of natural disaster damage. *Global Environmental Change* 2014; **24**:8–19.
3. Jalayer F, Cornell CA. A technical framework for probability-based demand and capacity factor design (DCFD) seismic formats. *PEER Report 2003/08*, Pacific Earthquake Engineering Research Center, College of Engineering, University of California, Berkeley, CA 2003.
4. Deierlein G, Krawinkler H, Cornell C. A framework for performance-based earthquake engineering. *Pacific conference on earthquake engineering*, Christchurch, New Zealand, 2003; 1–8.
5. Moehle J, Deierlein GG. A framework methodology for performance-based earthquake engineering. *13th World conference on earthquake engineering*, Vancouver, Canada, 2004; 3812–3814.
6. Conte J, Zhang Y. Performance based earthquake engineering: Application to an actual bridge-foundation-ground system. *12th Italian National Conference on Earthquake Engineering*, Pisa, Italy, 2007; 1–18.
7. Lange D, Devaney S, Usmani A. An application of the peer performance based earthquake engineering framework to structures in fire. *Engineering Structures* 2014; **66**:100–115.
8. Kılıç C, Ulusoy M. Psychological effects of the november 1999 earthquake in turkey: an epidemiological study. *Acta Psychiatrica Scandinavica* 2003; **108**(3):232–238.
9. Department of Homeland Security, FEMA, Washington DC. *Multi-Hazard Loss Estimation Methodology: Earthquake Model. HAZUS-MH 2.1. Technical Manual* 2011.
10. Bonabeau E. Agent-based modeling: Methods and techniques for simulating human systems. *Proceedings of the National Academy of Sciences of the United States of America* 2002; **99**(Suppl 3):7280–7287.
11. Poulos A. Risk model of human evacuation under earthquake loads. Master's Thesis, Pontifical Catholic University of Chile 2014.
12. Wilensky U. Netlogo. *http://ccl.northwestern.edu/netlogo/*, Center for Connected Learning and Computer-Based Modeling, Northwestern University, Evanston, IL 1999.
13. Dijkstra EW. A note on two problems in connexion with graphs. *Numerische mathematik* 1959; **1**(1):269–271.
14. Van Den Berg J, Guy SJ, Lin M, Manocha D. Reciprocal n-body collision avoidance. *Robotics Research*. Springer, 2011; 3–19.
15. Liu Z, Jalalpour M, Jacques C, Szyniszewski S, Mitrani-Reiser J, Guest J, Igusa T, Schafer B. Interfacing building response with human behavior under seismic events. *15th World Conference on Earthquake Engineering*, Lisbon, Portugal, 2012.
16. Pan X. Computational modeling of human and social behaviors for emergency egress analysis. PhD Thesis, Stanford University 2006.
17. Rinne T, Tillander K, Grönberg P. Data collection and analysis of evacuation situations. *Research Notes 2562*, VTT Technical Research Centre of Finland, Espoo, Finland 2010.
18. Fujiyama T, Tyler N. Pedestrian speeds on stairs: an initial step for a simulation model. *Proceedings of 36th Universities Transport Studies Group Conference*, Newcastle upon Tyne, UK, 2004.
19. Meister J. Simulation of crowd dynamics with special focus on building evacuations. Master's Thesis, University of Applied Sciences Wedel 2007.
20. Lomnitz C. Comment on "Temporal and magnitude dependence in earthquake recurrence models" by CA Cornell and SR Winterstein. *Bulletin of the Seismological Society of America* 1989; **79**(5):1662–1662.
21. Cornell CA. Engineering seismic risk analysis. *Bulletin of the Seismological Society of America* 1968; **58**(5):1583–1606.
22. Gutenberg B, Richter CF. Frequency of earthquakes in california. *Bulletin of the Seismological Society of America* 1944; **34**(4):185–188.
23. Alvarez M. Evaluación y predicción de daños sísmicos en estructuras convencionales y con SRV : implementación numérica [Assessment and prediction of seismic damage in conventional structures and with vibration control systems: a numerical implementation]. Master's Thesis, Pontifical Catholic University of Chile 2001.
24. Leyton F, Ruiz S, Sepúlveda S. Preliminary re-evaluation of probabilistic seismic hazard assessment in Chile: from Arica to Taitao Peninsula. *Advances in Geosciences* 2009; **22**(22):147–153.
25. Abrahamson N, Gregor N, Addo K. BC Hydro ground motion prediction equations for subduction earthquakes. *Earthquake Spectra* 2015; In-Press.
26. Baker JW, Cornell CA. Spectral shape, epsilon and record selection. *Earthquake Engineering & Structural Dynamics* 2006; **35**(9):1077–1095.
27. Baker JW. Conditional mean spectrum: Tool for ground-motion selection. *Journal of Structural Engineering* 2010; **137**(3):322–331.
28. Baker JW, Cornell CA. Correlation of response spectral values for multicomponent ground motions. *Bulletin of the Seismological Society of America* 2006; **96**(1):215–227.
29. Baker JW, Jayaram N. Correlation of spectral acceleration values from nga ground motion models. *Earthquake Spectra* 2008; **24**(1):299–317.
30. Clough RW, Penzien J. *Dynamics of structures*. 3 edn., Computers & Structures Inc.: Berkeley, CA, 2003.
31. COSMOS. Strong-motion virtual data center. URL http://strongmotioncenter.org/vdc, [accessed July 2015].
32. University of Chile, Department of Civil Engineering. Earthquakes of chile. URL http://terremotos.ing.uchile.cl, [accessed July 2015].
33. Bazzurro P, Cornell CA. Disaggregation of seismic hazard. *Bulletin of the Seismological Society of America* 1999; **89**(2):501–520.
34. Arias A. A measure of earthquake intensity. *Seismic Design for Nuclear Power Plants*, Hansen RJ (ed.). MIT Press: Cambridge, MA, 1970; 438–483.
35. McKenna F, Fenves G, Scott M, Jeremic B. Open system for earthquake engineering simulation (OpenSees). *Pacific earthquake engineering research center*, University of California, Berkeley, CA 2000.

DOI: 10.1002/eqe.2803

36. Scott MH, Fenves GL. Plastic hinge integration methods for force-based beam–column elements. *Journal of Structural Engineering* 2006; **132**(2):244–252.
37. Retamales R, Davies R, Mosqueda G, Filiatrault A. Experimental seismic fragility of cold-formed steel framed gypsum partition walls. *Journal of Structural Engineering* 2013; **139**(8):1285–1293.
38. Badillo-Almaraz H, Whittaker AS, Reinhorn AM. Seismic fragility of suspended ceiling systems. *Earthquake Spectra* 2007; **23**(1):21–40.
39. Echevarria A, Zaghi A, Soroushian S, Maragakis M. Seismic fragility of suspended ceiling systems. *15th World Conference on Earthquake Engineering*, Lisbon, Portugal, 2012.
40. Epstein B, Lomnitz C. A model for the occurrence of large earthquakes. *Nature* 1966; **211**:954–956.
41. Der Kiureghian A. Non-ergodicity and PEER's framework formula. *Earthquake engineering & structural dynamics* 2005; **34**(13):1643–1652.
42. Yeo GL, Cornell CA. Building life-cycle cost analysis due to mainshock and aftershock occurrences. *Structural Safety* 2009; **31**(5):396–408.
43. Cutfield M, Ma Q. Probability distributions of cumulative losses caused by earthquakes. *15th World Conference on Earthquake Engineering*, Lisbon, Portugal, 2012.
44. Taghavi S, Miranda E. Response assessment of nonstructural building elements. *PEER Report 2003/05*, Pacific Earthquake Engineering Research Center, College of Engineering, University of California, Berkeley, CA 2003.
45. James F. Monte carlo theory and practice. *Reports on Progress in Physics* 1980; **43**(9):1145.
46. Weinzierl S. Introduction to monte carlo methods. *ArXiv High Energy Physics - Phenomenology e-prints* 2000; URL http://arxiv.org/abs/hep-ph/0006269v1.

DOI: 10.1002/eqe.2803